Chemical Bonding in Hypervalent Molecules Revised. Application of the *Atoms in Molecules Theory* to Y_3X and Y_3XZ (Y = H or CH_3; X = N, P or As; Z = O or S) Compounds

J. A. Dobado,[†] Henar Martínez-García,[†] José Molina Molina,*[,†] and Markku R. Sundberg*[,‡]

Contribution from the Grupo de Modelización y Diseño Molecular, Instituto de Biotecnología, Campus Fuentenueva, Universidad de Granada, E-18071 Granada, Spain, and Laboratory of Inorganic Chemistry, Department of Chemistry, P.O. Box 55 (A.I. Virtasen aukio 1), FIN-00014 University of Helsinki, Finland

Received January 13, 1998. Revised Manuscript Received June 8, 1998

Abstract: *Atoms in Molecules Theory* has been applied to analyze bonding properties, in potentially hypervalent pnicogen (N, P or As)−chalcogen(O or S) bonds within the framework of three plausible models: (*i)* one σ bond and two π back-bonds (negative hyperconjugation), (*ii)* one σ bond and three π back-bonds, and (*iii)* three Ω (banana) bonds. The topological analyses (based upon the electron charge density ($\rho(r)$), its Laplacian ($\nabla^2\rho(r)$), bond ellipticity, etc.) and the charges were consistent with a highly polarized σ bond, with bond strength dependent on the electrostatic interactions. The equilibrium geometries were optimized by both density functional theory with a hybrid functional (B3LYP) and by ab initio methods at the MP2(full) level, using the 6-311G basis set augmented by polarization and/or diffuse functions.

I. Introduction

During the past few years, there has been widespread interest in hypervalent phosphorus compounds, focusing on the nature of the bond in phosphine oxides[1−12] and thiophosphenes.[12−14] Moreover, the P−O bond has been of general interest, and it has been studied in general reviews;[15] however, there are still several points of controversy in the P−O bond description. The combined experimental evidence[15,16] is that the phosphoryl bond is strong, short, and polar, and, while the sulfur analogues are similar, they are not quite as strong. Thus, the P−O bond order is said to be greater than 2 and the P−S bond somewhat less than 2.[15] For years, the description of the structure and bonding in phosphorus compounds was connected with the concept of the involvement of virtual d orbitals in P−O bonding studies. Nevertheless, there are several pieces of theoretical evidence against this involvement.[2,17−28] More recently, Gilheany provided an extensive discussion of whether d orbitals are involved in the bonding of hypervalent molecules.[16] After a detailed review of the subject, the conclusion was that d orbitals are not involved. The nature of the P−O bond has been extensively reviewed over the years;[29−39] in general, its nature has been explained in terms of a combination of two different descriptions

* Correspondence may be addressed to the authors via e-mail: jmolina@goliat.ugr.es, sundberg@cc.helsinki.fi.

† Universidad de Granada.

‡ University of Helsinki.

(1) Wallmeier, H.; Kutzelnigg, W. *J. Am. Chem. Soc.* **1979**, *101*, 2804.
(2) Kutzelnigg, W. *Angew. Chem., Int. Ed. Engl.* **1984**, *23*, 272.
(3) Kutzelnigg, W. *Pure Appl. Chem.* **1977**, *49*, 981.
(4) Bollinger, J. C.; Houriet, R.; Kern, C. W.; Perret, D.; Weber, J.; Yvernault, T. *J. Am. Chem. Soc.* **1985**, *107*, 5352.
(5) Keil, F.; Kutzelnigg, W. *J. Am. Chem. Soc.* **1975**, *97*, 3623.
(6) Messmer, R. P. *J. Am. Chem. Soc.* **1991**, *113*, 433.
(7) Gordon, M. S.; Boatz, J. A.; Schmidt, M. W. *J. Phys. Chem.* **1984**, *88*, 2998.
(8) Schmidt, M. W.; Gordon, M. S. *J. Am. Chem. Soc.* **1985**, *107*, 1922.
(9) Boatz, J. A.; Gordon, M. S. *J. Comput. Chem.* **1986**, *7*, 306.
(10) Streitwieser, A.; McDowell, R. S.; Glaser, R. *J. Comput. Chem.* **1987**, *8*, 788.
(11) Streitwieser, A.; Rajca, A.; McDowell, R. S.; Glaser, R. *J. Am. Chem. Soc.* **1987**, *109*, 4184.
(12) Schneider, W.; Thiel, W.; Komornicki, A. *J. Phys. Chem.* **1988**, *92*, 5611.
(13) Maclagan, R. *J. Phys. Chem.* **1990**, *94*, 3373.
(14) Liang, C.; Allen, L. C. *J. Am. Chem. Soc.* **1987**, *109*, 6449.
(15) Gilheany, D. G. *The Chemistry of Organophosphorous Compounds*; Wiley-Interscience: Chichester, 1992; Vol. 2.
(16) Gilheany, D. G. *Chem. Rev.* **1994**, *94*, 1339.
(17) Kutzelnigg, W. *J. Mol. Struct. THEOCHEM* **1988**, *46*, 403.
(18) Ehrhardt, C.; Ahlrichs, R. *Theor. Chim. Acta* **1985**, *68*, 231.
(19) Heinzmann, R.; Ahlrichs, R. *Theor. Chim. Acta* **1976**, *42*, 33.
(20) Cruickshank, D. W. J.; Eisenstein, M. *J. Mol. Structure* **1985**, *130*, 143.
(21) Cruickshank, D. W. J. *J. Mol. Structure* **1985**, *130*, 177.
(22) Cruickshank, D. W. J.; Eisenstein, M. *J. Comput. Chem.* **1987**, *8*, 6.
(23) Reed, A. E.; Weinhold, F. *J. Am. Chem. Soc.* **1986**, *108*, 3586.
(24) Reed, A. E.; Schleyer, P. v. R. *Chem. Phys. Lett.* **1987**, *133*, 553.
(25) Foster, J. P.; Weinhold, F. *J. Am. Chem. Soc.* **1980**, *102*, 7211.
(26) Reed, A. E.; Weinstock, R. B.; Weinhold, F. *J. Chem. Phys.* **1985**, *83*, 735.
(27) Reed, A. E.; Weinhold, F. *J. Chem. Phys.* **1985**, *83*, 1736.
(28) Reed, A. E.; Curtiss, L. A.; Weinhold, F. *Chem. Rev.* **1988**, *88*, 899.
(29) Mitchell, K. A. R. *Chem. Rev.* **1969**, *69*, 157.
(30) Hudson, R. F. *Structure and Mechanism in Organophosphorous Chemistry;* Academic Press: London, 1965.
(31) Kirby, A. J.; Warren, S. G. *The Organic Chemistry of Phosphorus;* Elsevier: Amsterdam, 1967.
(32) Walker, B. J. *Organophosphorus Chemistry;* Penguin: Hardmondsworth, 1972.
(33) Corbridge, D. E. C. *The Structural Chemistry of Phosphorus;* Elsevier: Amsterdam, 1974.
(34) Emsley, J.; Hall, D. *The Chemistry of Phosphorus;* Harper and Row: London, 1976.
(35) Goldwhite, H. *Introduction to Phosphorus Chemistry;* Cambridge University Press: Cambridge, 1981.
(36) Corbridge, D. E. C. *Phosphorus, an Outline of its Chemistry, Biochemistry and Technology;* Elsevier: Amsterdam, 1985.
(37) Hays, H. R.; Peterson, D. J. *Organic Phosphorus Compounds;* Wiley-Interscience: Chichester, 1972.
(38) Maier, L. *Organic Phosphorus Compounds;* Wiley-Interscience: Chichester, 1972; Vol. 4, Chapter 7, pp 1−73.

S0002-7863(98)00141-3 CCC: $15.00
Published on Web 08/05/1998

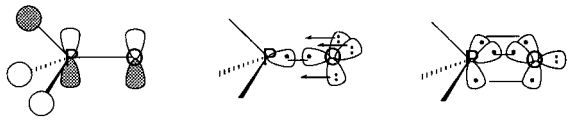

Figure 1. Representation of the three proposed P−O bonding schemes.

via a resonance between structures **a** and **b**:

$$\underset{\mathbf{a}}{R_3P^+-O^-} \leftrightarrow \underset{\mathbf{b}}{R_3P=O}$$

Structure **a** obeys the octet rule, but some back electron donation is necessary from oxygen to phosphorus, allowing structure **b** to contribute. This scheme has been discussed over the last 15 years, and Gilheany has recently reviewed[16] the different possibilities which arise from the above **a** ↔ **b** hybrid, also pointing out the difficulty in such a description. Moreover, the following three alternatives were considered to describe the P−O bonding:

i. One σ Bond and Two π Back-Bonds (Negative Hyperconjugation). The bond is considered to be a donor−acceptor interaction with superimposed back-bonding.[7,8,40] The lone pair from phosphorus forms a σ bond to oxygen. The resulting extra charge density on oxygen may go into acceptor orbitals on phosphorus, forming a double or partial triple bond, by a π-type interaction (back-bonding)[1,2,41] (see Figure 1a). The suitable orbitals of phosphorus, from this interaction, are a set of antibonding orbitals of *e* symmetry on the Y_3 P moiety.

ii. One σ Bond and Three π Back-Bonds. This view is essentially structure **a** with some polarization of the charge toward each of the atoms involved.[10,11] There is some uncertainty about the interpretation of this polarization as (a) back-bonding or (b) charge polarization in an ionic bond. The representation of this bonding scheme is presented in Figure 1b. Schmidt et al.[42] agree with the three π back-bonding scheme, from an energy localization point of view. Seen in this way, there is one σ P−O bond and three equivalent orbitals on oxygen, staggered with the three substituents of phosphorus. This staggered conformation is inconsistent with the negative hyperconjugation alternative i which would have an eclipsed conformation.

iii. Three Ω Bonds (Banana Bonds). There are neither σ nor π bonds, but the P−O bond is a formal triple bond with the three curved regions of electron density placed between P and O in a symmetrical fashion (see Figure 1c). As it is displayed in Figure 1c, the remaining lone pair on the oxygen atom points away from phosphorus along the P−O axis. The "banana bond" description suggests itself for the phosphine oxide derivatives, on one hand from a Boys localization scheme[1,42−44] and on the other from generalized valence bond calculations.[6,45−47]

Debate about the above three schemes continues. The arguments for the three possibilities arose from different analyses of the theoretical wavefunction, as pointed out in Gilheany's review.[16] For example, an energy localization procedure of the H_3 PO theoretical calculations gives a representation compatible with scheme ii, and the Boys localization of the same theoretical calculations gives orbital representation compatible with the "banana bond" (iii).[42] The NBO analysis of the HF and MP2 calculations on hypervalent molecules induced Schleyer to propose the negative hyperconjugative scheme i.[41] The same alternative was supported by Ziegler and co-workers for different chalcogenide bonds from a general energy decomposition scheme using different virtual orbitals in the calculation.[48] However, Power et al.,[49] from experimental and theoretical studies on phosphorus chemical shielding tensors in R_3 PX compounds (X = BH_3, CH_2, NH or O), concluded that the P−O bonding is purely dative in nature with no multiple bond character detectable from the nuclear magnetic shielding.

Bader's theory is now used to describe many different types of compounds.[50−52] Among these are the phosphonic acid derivatives.[53,54] In our group the *Atoms in Molecules Theory* has also been used in the field of intermolecular interactions[55,56] and transition metal complexes.[57,58] The literature contains many theoretical calculations on these systems studied[15,41,48,59,60] (compounds **1**−**24**, see Figures 2 and 3), with results usually in good agreement with the experimental geometries. In the present and in following papers the nature of the hypervalent X−Y bonds (X = N, P, As, O, S or Se; Y = O, S or CH_2) is revised in the framework of Bader's theory. In this work, special emphasis will be placed on the nature of the P−O bond based upon the proposed theoretical alternatives: i−iii.

II. Methods of Calculation

A. General Methods. Density functional theory (DFT, using the hybrid Becke 3-Lee−Yang−Parr (B3LYP) exchange-correlation functional[61,62]) and the full second-order Møller−Plesset MP2(full)[63] calculations were carried out with the Gaussian 94 package of programs,[64] using 6-311G* and 6-311+G* basis sets. All the structures presented were fully optimized, with constrained C_{3v} symmetry for **1**−**19** and C_s for **20**−**24**. To test the validity of these symmetry restrictions, full geometry optimizations were performed for **7** (H_3 NO), **11** (H_3 PO), **12** (Me_3 PO), and **19** (F_3 NO), starting from different distorted geometries. The numerical results obtained from the non-symmetrical calculations yielded the same geometries (within <0.001

(39) Smith, D. J. H. *Comprehensive Organic Chemistry;* Pergamon: Oxford, 1979; Vol. 2, pp 1121−1122.
(40) Schmidt, M. W.; Gordon, M. S. *Can. J. Chem.* **1985**, *63*, 1609.
(41) Reed, A. E.; Schleyer, P. v. R. *J. Am. Chem. Soc.* **1990**, *112*, 1434.
(42) Schmidt, M. W.; Yabushita, S.; Gordon, M. S. *J. Phys. Chem.* **1984**, *88*, 382.
(43) Guest, M. F.; Hillier, I. H.; Saunders: V. R. *J. Chem. Soc., Faraday Trans. 2* **1972**, 867.
(44) Molina, P.; Alajarin, M.; Leonardo, C. L.; Claramunt, R. M.; Foces-Foces, M. D. L. C.; Cano, F. H.; Catalán, J.; de Paz, J. L. G.; Elguero, J. *J. Am. Chem. Soc.* **1989**, *111*, 355.
(45) Schultz, P. A.; Messmer, R. P. *J. Am. Chem. Soc.* **1993**, *115*, 10925.
(46) Schultz, P. A.; Messmer, R. P. *J. Am. Chem. Soc.* **1993**, *115*, 10938.
(47) Murphy, R. B.; Messmer, R. P. *J. Chem. Phys.* **1993**, *98*, 7958.
(48) Sandblom, N.; Ziegler, T.; Chivers, T. *Can. J. Chem.* **1996**, *74*, 2363.
(49) Power, W. P. *J. Am. Chem. Soc.* **1995**, *117*, 1800.
(50) Fan, M. F.; Jia, G. C.; Lin, Z. Y. *J. Am. Chem. Soc.* **1996**, *118*, 9915.
(51) Platts, J. A.; Howard, S. T.; Bracke, B. R. F. *J. Am. Chem. Soc.* **1996**, *118*, 2726.
(52) Heinemann, C.; Muller, T.; Apeloig, Y.; Schwarz, H. *J. Am. Chem. Soc.* **1996**, *118*, 2023.
(53) Hernández-Laguna, A.; Sainz-Díaz, C. I.; Smeyers, Y. G.; de Paz, J. L. G.; Gálvez Ruano, E. *J. Phys. Chem.* **1994**, *98*, 1109.
(54) Sainz-Díaz, C. I.; Hernández-Laguna, A.; Smeyers, Y. G. *J. Mol. Struct. THEOCHEM* **1997**, *390*, 127.
(55) Dobado, J. A.; Molina, J. *J. Phys. Chem.* **1994**, *98*, 1819.
(56) Dobado, J. A.; Portal, D.; Molina, J. *J. Phys. Chem. A* **1998**, *102*, 778.
(57) Navarro, J. A. R.; Romero, M. A.; Salas, J. M.; Quiros, M.; El-Bahraoui, J.; Molina, J. *Inorg. Chem.* **1996**, *35*, 7829.
(58) El-Bahraoui, J.; Molina, J.; Portal, D. *J. Phys. Chem. A* **1998**, *102*, 2443.
(59) Yang, C.; Goldstein, E.; Breffle, S.; Jin, S. *J. Mol. Struct. THEOCHEM* **1992**, *259*, 345.
(60) Pacchioni, G.; Bagus, P. S. *Inorg. Chem.* **1992**, *31*, 4391.
(61) Lee, C.; Yang, W.; Parr, R. G. *Phys. Rev. B* **1988**, *37*, 785.
(62) Becke, A. D. *J. Chem. Phys.* **1993**, *98*, 5648.
(63) Møller, C.; Plesset, M. S. *Phys. Rev.* **1934**, *46*, 618.

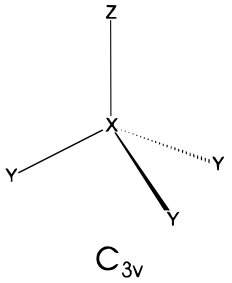

	X	Y	Z
1	N	H	-
2	N	Me	-
3	P	H	-
4	P	Me	-
5	As	H	-
6	As	Me	-
7	N	H	O
8	N	Me	O
9	N	H	S
10	N	Me	S
11	P	H	O
12	P	Me	O
13	P	H	S
14	P	Me	S
15	As	H	O
16	As	Me	O
17	As	H	S
18	As	Me	S
19	N	F	O

Figure 2. Hypervalent structures **1**−**19**.

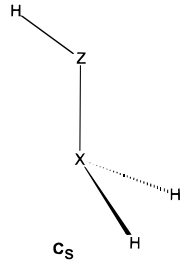

	X	Z
20	P	O
21	P	S
22	As	O
23	As	S
24	N	S

Figure 3. Structures **20**−**24**.

Å for bond lengths and <0.1° for bond and torsion angles). Full Bader analyses have also been performed for the nonsymmetrical structures, giving numerical values for ρ(r) and $\nabla^2\rho(r)$ at the critical points of ρ(r) and $\nabla^2\rho(r)$ within <0.002. In addition, the calculated charges differ by <0.02. A vibrational analysis was used to check the nature of the stationary points, and none of the structures **1**−**24** presented imaginary frequencies (true minima) at both B3LYP and MP2 levels with the 6-311+G* basis. The Bader analyses have been performed with the AIMPAC series of programs[65] using the DFT and MP2 wavefunctions as input, as was described in *Atoms in Molecules Theory*.[66,67] The $\nabla^2\rho(r)$ contour map representations of the different structures were obtained using the MORPHY program.[68] The atomic charges have been calculated using the AIMPAC series of programs,[65] by integration over the basin of every atom in the Bader's framework.

B. Overview of the *Atoms in Molecules Theory*. The topology of the electronic charge density ($\rho(r)$), as pointed out by Bader,[66] is an accurate mapping of the chemical concepts of atom, bond, and structure. The principal topological properties are summarized in terms of their critical points (CP).[66,67] The nuclear positions behave topologically as local maxima in $\rho(r)$. A bond-critical point (BCP) is found between each pair of nuclei, which are considered to be linked by a chemical bond, with two negative curvatures (λ_1 and λ_2) and one positive (λ_3) (denoted as (3,−1) CP). The ellipticity (ϵ) of a bond is defined by means of the two negative curvatures in a BCP as

$$\epsilon = \lambda_1/\lambda_2 - 1 \qquad (1)$$

where $|\lambda_2| < |\lambda_1|$. The ring CPs are characterized by a single negative curvature. Each (3,−1) CP generates a pair of gradient paths[66] which originate at a CP and terminate at neighboring attractors. This gradient path defines a line through the charge distribution linking the neighboring nuclei. Along this line, $\rho(r)$ is a maximum with respect to any neighboring line. Such a line is referred to as an atomic interaction line.[66,67] The presence of an atomic interaction line in such equilibrium geometry satisfies both the necessary and sufficient condition that the atoms be bonded together.

The Laplacian of the electronic charge density ($\nabla^2\rho(r)$) describes two extreme situations. In the first $\rho(r)$ is locally concentrated ($\nabla^2\rho(r) < 0$) and in the second is locally depleted ($\nabla^2\rho(r) > 0$). Thus, a value of $\nabla^2\rho(r) < 0$ at a BCP is unambiguously related to a covalent bond, showing that a sharing of charge has taken place. While, in a closed-shell interaction a value of $\nabla^2\rho(r) > 0$ is expected, as found in noble gas repulsive states, in ionic bonds, in hydrogen bonds, and in van der Waals molecules.

Bader has also defined a local electronic energy density ($E_d(r)$), as a functional of the first-order density matrix:

$$E_d(r) = G(r) + V(r) \qquad (2)$$

where the $G(r)$ and $V(r)$ correspond to a local kinetic and potential energy density, respectively.[66] The sign of the $E_d(r)$ determines whether accumulation of charge at a given point r is stabilizing ($E_d(r) < 0$) or destabilizing ($E_d(r) > 0$). Thus, a value of $E_d(r) < 0$ at a BCP presents a significant covalent contribution and, therefore, a lowering of the potential energy associated with the concentration of charge between the nuclei. Very recently, for some saturated and unsaturated hydrocarbons, Grimme[69] has found a linear correlation between the bond energies, the $E_d(r)$ and ρ(r) at the position of the BCPs.[70]

III. Results and Discussion

A. General Considerations and Geometrical Description. From the literature,[16,71] we find that the theoretical description of hypervalent molecules agrees with the experimental data when polarization functions are added to the basis set. Results are also improved by the inclusion of electron correlation.[16,72] From the calculations indicated in previous section, we present only the results comparing the DFT and MP2(full) methods using the 6-311+G* basis set.[73] The numerical results obtained are presented in Tables 1−5. Table 1 shows the theoretical and experimental geometrical parameters. Table 2 presents the numerical properties of the different BCPs in $\rho(r)$ while the numerical properties of the maxima of $\nabla^2\rho(r)$ (maxima in electron density concentration) in the valence shell charge concentration (VSCC) for the different atoms are presented in Table 3. Table 4 includes the atomic charges obtained from Bader's methodology and the dipole moments. Finally, Table 5 lists the Total energies (Hartrees), and it is available as Supporting Information. The geometrical parameters calculated

(64) Frisch, M. J.; Trucks, G. W.; Schlegel, H. B.; Gill, P. M. W.; Johnson, B. G.; Robb, M. A.; Cheeseman, J. R.; Keith, T.; Petersson, G. A.; Montgomery, J. A.; Raghavachari, K.; Al-Laham, M. A.; Zakrzewski, V. G.; Ortiz, J. V.; Foresman, J.; Cioslowski, B. B.; Stefanov, A.; Nanayakkara, M.; Challacombe, J. B.; Peng, C. Y.; Ayala, P. Y.; Chen, W.; Wong, M. W.; Andres, J. L.; Replogle, E. S.; Gomperts, R.; Martin, R. L.; Fox, D. J.; Binkley, J. S.; Defrees, D. J.; Baker, J.; Stewart, J. J. P.; Head-Gordon, M.; Gonzalez, C.; Pople, J. A. *Gaussian 94*, revision C.2; Gaussian Inc.: Pittsburgh, PA, 1995.

(65) Biegler-Koning, F. W.; Bader, R. F. W.; Tang, T. H. *J. Comput. Chem.* **1982**, *3*, 317.

(66) Bader, R. F. W. *Atoms in Molecules: a quantum theory;* Clarendon Press: Oxford, 1990.

(67) Bader, R. F. W. *Chem. Rev.* **1991**, *91*, 893.

(68) Popelier, P. L. A. *Comput. Phys. Commun.* **1996**, *93*, 212.

(69) Grimme, S. *J. Am. Chem. Soc.* **1996**, *118*, 1529.

(70) $E_d(r)$ values (hartree/bohr^3) for several covalent and ionic molecules are $H_2 = -0.262$, $N_2 = -1.54$, $CH_4 = -0.262$, HF = −0.588, HLi = 0.0012.

(71) For example, see ref 80, p 185.

(72) Yates, B. F.; Bouma, W. J.; Radom, L. *J. Am. Chem. Soc.* **1987**, *109*, 2250.

(73) Results using the 6-311G* basis are available upon request from the authors.

Table 1. Geometrical Parameters (Å and deg) for Structures **1**−**24** at the Different Theoretical Levels

	Z−X			X−Y			∠Z−X−Y[a]			∠Y−X−Y		
	DFT	MP2	exp	DFT	MP2	exp	DFT	MP2	exp	DFT	MP2	exp
1 (H_3N)				1.014	1.010	1.012[b]	110.9	110.4		107.9	108.5	106.7[b]
2 (Me_3N)				1.454	1.452	1.451[c,d]	107.1	108.2		111.7	110.7	110.9[c,d]
3 (H_3P)				1.423	1.414	1.4215[e,d]	122.9	121.9		93.4	94.6	93.36[e,d]
4 (Me_3P)				1.862	1.845	1.847[f,g]	118.4	118.9	118.9[f,g]	99.3	98.6	98.6[f,g]
5 (H_3As)				1.530	1.521	1.511[b]	123.9	123.5		91.8	92.5	92.1[b]
6 (Me_3As)				1.989	1.963	1.964[h,g]	120.1	120.5		97.0	96.5	96.0[h,g]
7 (H_3NO)	1.365	1.360		1.033	1.027		113.1	112.5		105.7	106.3	
8 (Me_3NO)	1.367	1.361	1.388[i,j]	1.501	1.489	1.479[i,j]	109.6	109.6	109.9[i,j]	109.3	109.4	109.1[i,j]
			1.379[k,j]			1.496[k,j]			108.9[k,j]			110.0[k,j]
9 (H_3NS)	1.866	1.842		1.017	1.016		110.9	110.9		108.1	108.1	
10 (Me_3NS)	1.858	1.823		1.493	1.486		109.4	109.6		109.5	109.4	
11 (H_3PO)	1.492	1.491		1.419	1.411		117.1	117.0		101.0	100.9	
12 (Me_3PO)	1.500	1.500	1.476[l,g]	1.830	1.813	1.809[l,g]	113.8	114.0	114.4[l,g]	104.9	104.6	104.1[l,g]
			1.489[m,j]			1.771[m,j]			113.1[m,j]			105.9[m,j]
13 (H_3PS)	1.957	1.941		1.417	1.408		118.0	117.7		99.8	100.2	
14 (Me_3PS)	1.972	1.953	1.940[l,g]	1.835	1.816	1.818[l,g]	114.3	114.3	114.1[l,g]	104.2	104.2	104.5[l,g]
			1.959[n,j]			1.798[n,j]			113.2[n,j]			105.8[n,j]
15 (H_3AsO)	1.646	1.640		1.523	1.517		116.3	116.4		101.9	101.8	
16 (Me_3AsO)	1.653	1.648	1.631[l,g]	1.956	1.929	1.937[l,g]	113.6	114.1	112.6[l,g]	105.0	104.4	106.2[l,g]
17 (H_3AsS)	2.083	2.064		1.521	1.513		117.4	117.4		100.5	100.5	
18 (Me_3AsS)	2.095	2.074	2.059[l,g]	1.958	1.929	1.940[l,g]	114.5	114.7	113.4[l,g]	104.0	103.8	105.2[l,g]
19 (F_3NO)	1.154	1.147	1.159[o,g,d]	1.445	1.447	1.432[o,g,d]	117.4	117.8	117.4[o,g,d]	100.5	100.1	100.5[o,g,d]

	Z−X		X−H		∠Z−X−H		∠X−Z−H		Z−H	
	DFT	MP2	DFT	MP2	DFT	MP2	DFT	MP2	DFT	MP2
20 (H_2POH)	1.684	1.676	1.422	1.413	97.8	99.1	111.9	112.3	0.966	0.960
21 (H_2PSH)	2.168	2.132	1.420	1.410	97.1	98.0	94.9	95.1	1.353	1.341
22 (H_2AsOH)	1.836	1.824	1.533	1.523	94.9	95.4	109.6	109.4	0.968	0.963
23 (H_2AsSH)	2.288	2.256	1.530	1.522	94.9	95.7	94.1	93.8	1.351	1.344
24 (H_2NSH)	1.732	1.716	1.010	1.009	110.9	111.6	97.1	97.0	1.358	1.346

[a] For **1**−6, ∠Z−X−Y is the angle formed with the C_3 symmetry axis. [b] Taken from ref 80, page 138. [c] Reference 81. [d] Microwave spectroscopy data. [e] Reference 82. [f] Reference 83. [g] Electron diffraction data. [h] Reference 84. [i] Reference 85. [j] X-ray crystallography at room temperature. [k] Reference 86. [l] Reference 79. [m] Reference 87. [n] Reference 88. [o] Reference 89.

for compounds **1**−**24**, listed in Table 1, in general agree with earlier theoretical calculations or experimental determinations, taking into account the different experimental data available and the possible source of error in the comparison of theoretical and experimental equilibrium geometries.[74] The following geometrical trends were easily extracted from Table 1:

● The P−O bond in phosphine oxides was always considerably shorter than the standard P−O single bond; thus, values smaller than 1.5 Å were obtained in comparison with 1.6 Å for a standard P−O single bond (e.g. ∼1.68 Å was obtained for compound **20**).

● The P−S bond was shorter than the standard P−S single bond (1.95−1.97 Å in **13** compared with 2.13−2.17 Å in **21**).

● In a similar way, the As−O (∼1.64−1.65 vs 1.83 Å) and As−S (∼2.06−2.09 vs 2.28 Å) bonds were also shorter than their respective standard bonds.

● The N−O bond in amine oxides corresponds to the standard single bond, as was pointed out elsewhere,[16] but it decreases significantly when the hydrogens are substituted by fluorine (1.36 Å vs 1.15 Å).

● The ∠Y−X−Y angles increased passing from phosphine, arsine, to the corresponding oxides or sulfur derivatives.

B. Nature of the P−O Bond. As we mention in the Introduction there are three possible distributions for the PO bond in phosphine oxides, referred to as i, ii, and iii, two of which involve the location of electron density along the P−O internuclear axis, while the other does not. Until now, the discussion of these three possibilities has dealt in general with different types of wavefunction analyses, yielding contradictory results (see Introduction). This possible controversy between the different wavefunction analyses was pointed out Cioslowski et al.,[75,76] "in the interpretation and analysis of the electronic wavefunction one should apply only observable-based tools". Currently, there is only one general approach available which provides a comprehensive set of observable-based interpretative tools (the topological theory of atoms in molecules). Therefore, in our bonding studies, we are using as alternative the topological analysis of $\rho(r)$ due to Bader.[66,67] This analysis has the advantage of being done from a $\rho(r)$ that has a physical meaning, and, if the starting wavefunction is accurate enough, it becomes basis set independent.

Considering the three bonding possibilities (i−iii) (see Figure 1**a**−**c**), the expected Bader results for all them were compared with those obtained in this work. For the possibilities i and ii, some electron density concentration along the P−O bond is expected, but for iii there must be no electron density concentration along the P−O internuclear axis. Nevertheless, for iii there must be a maximum of electron density concentration in P−O region away from the O atom which should be revealed by the $\nabla^2\rho(r)$ topology. Schemes i and ii differ in the orientation of the nonbonded electron density concentration around the oxygen. For i, there must be one maximum of electron density concentration on oxygen, coplanar with one of the substituents of phosphorus while for ii all three maxima of electron density concentration should be equivalent, symmetrically oriented, and staggered with respect to the bonds to the other phosphorus ligands. The nature of the atomic interactions on formation of

(74) For example, see ref 80, p 137.

(75) Cioslowski, J.; Surján, P. R. *J. Mol. Struct. THEOCHEM* **1992**, *255*, 9.

(76) Cioslowski, J.; Mixon, S. T. *Inorg. Chem.* **1993**, *32*, 3209.

Table 2. Electronic Charge Density ($\rho(r)$), Its Laplacian ($\nabla^2\rho(r)$), Ellipticity (ϵ), Electronic Energy Density $E_d(r)$ and (λ_1/λ_3), at the Different Theoretical Levels[a] for the X−Z and X−Y BCPs[b] of Structures **1**−**19**

	1 H_3N	**3** H_3P	**5** H_3As	**7** H_3NO	**9** H_3NS	**11** H_3PO	**13** H_3PS	**15** H_3AsO	**17** H_3AsS
					$\rho(r)$ (e/a_o^3)				
B3LYP				0.342	0.127	0.225	0.163	0.206	0.131
	(0.331)	(0.159)	(0.138)	(0.328)	(0.335)	(0.170)	(0.169)	(0.146)	(0.146)
MP2				0.347	0.130	0.221	0.166	0.205	0.135
	(0.332)	(0.160)	(0.139)	(0.331)	(0.333)	(0.171)	(0.170)	(0.147)	(0.147)
					$\nabla^2\rho(r)$ (e/a_o^5)				
B3LYP				−0.226	−0.016	1.331	−0.235	0.557	−0.040
	(−1.454)	(−0.196)	(−0.098)	(−1.484)	(−1.629)	(−0.257)	(−0.259)	(−0.148)	(−0.145)
MP2				−0.274	−0.011	1.381	−0.262	0.618	−0.046
	(−1.549)	(−0.143)	(−0.099)	(−1.620)	(−1.711)	(−0.194)	(−0.202)	(−0.149)	(−0.147)
					ϵ				
B3LYP				0.000	0.000	0.000	0.000	0.000	0.000
	(0.036)	(0.092)	(0.030)	(0.011)	(0.007)	(0.074)	(0.025)	(0.025)	(0.009)
MP2				0.000	0.000	0.000	0.000	0.000	0.000
	(0.035)	(0.113)	(0.034)	(0.011)	(0.006)	(0.067)	(0.020)	(0.026)	(0.009)
					E_r				
B3LYP				−0.291	−0.087	−0.168	−0.115	−0.138	−0.069
	(−0.417)	(−0.156)	(−0.089)	(−0.414)	(−0.450)	(−0.177)	(−0.174)	(−0.097)	(−0.097)
MP2				−0.318	−0.102	−0.164	−0.126	−0.142	−0.076
	(−0.447)	(−0.162)	(−0.093)	(−0.454)	(−0.477)	(−0.182)	(−0.180)	(−0.102)	(−0.102)
					λ_1/λ_3				
B3LYP				0.587	0.534	0.181	1.643	0.266	0.596
MP2				0.607	0.526	0.176	2.084	0.255	0.612

	2 Me_3N	**4** Me_3P	**6** Me_3As	**8** Me_3NO	**10** Me_3NS	**12** Me_3PO	**14** Me_3PS	**16** Me_3AsO	**18** Me_3AsS	**19** F_3NO
					$\rho(r)$ (e/a_o^3)					
B3LYP				0.349	0.137	0.223	0.163	0.204	0.132	0.596
	(0.269)	(0.153)	(0.129)	(0.247)	(0.245)	(0.167)	(0.166)	(0.140)	(0.139)	(0.273)
MP2				0.353	0.145	0.220	0.166	0.204	0.136	0.599
	(0.269)	(0.154)	(0.134)	(0.252)	(0.247)	(0.168)	(0.167)	(0.147)	(0.145)	(0.269)
					$\nabla^2\rho(r)$ (e/a_o^5)					
B3LYP				−0.293	−0.063	1.291	−0.255	0.559	−0.046	−1.528
	(−0.696)	(−0.220)	(−0.056)	(−0.594)	(−0.589)	(−0.225)	(−0.256)	(−0.096)	(−0.095)	(0.083)
MP2				−0.326	−0.073	1.340	−0.287	0.612	−0.050	−1.567
	(−0.718)	(−0.105)	(−0.050)	(−0.635)	(−0.606)	(−0.096)	(−0.123)	(−0.092)	(−0.093)	(0.112)
					ϵ					
B3LYP				0.000	0.000	0.000	0.000	0.000	0.000	0.000
	(0.058)	(0.128)	(0.038)	(0.034)	(0.006)	(0.046)	(0.004)	(0.021)	(0.008)	(0.013)
MP2				0.000	0.000	0.000	0.000	0.000	0.000	0.000
	(0.051)	(0.142)	(0.042)	(0.039)	(0.011)	(0.042)	(0.003)	(0.021)	(0.008)	(0.013)
					E_r					
B3LYP				−0.305	−0.098	−0.168	−0.117	−0.137	−0.069	−0.899
	(−0.287)	(−0.146)	(−0.071)	(−0.251)	(−0.260)	(−0.171)	(−0.167)	(−0.082)	(−0.081)	(−0.185)
MP2				−0.332	−0.121	−0.164	−0.130	−0.140	−0.077	−0.957
	(−0.308)	(−0.151)	(−0.081)	(−0.283)	(−0.285)	(−0.172)	(−0.172)	(−0.096)	(−0.094)	(−0.192)
					λ_1/λ_3					
B3LYP				0.613	0.640	0.186	1.791	0.264	0.612	1.023
MP2				0.626	0.685	0.180	2.552	0.254	0.623	1.075

[a] All using 6-311+G* basis set as described in Methods section. [b] Values in parentheses corresponded to the X−Y BCPs.

a chemical bond can be analyzed in relation to the numerical values of the corresponding critical points. The *covalent interactions* are defined by large $\rho(r)$ values in the bond region, also giving large and negative values of $\nabla^2\rho(r)$. For the *ionic bonds* the $\rho(r)$ is very small and depleted on the bond region, giving positive $\nabla^2\rho(r)$ values. Thus, we are going to use these numerical properties, obtained at the corresponding BCPs, for the investigation of the P−O bond. For comparison, the parent compounds **1**−**6** proved to be covalent molecules with an electron concentration in the bond region, giving large values of $\rho(r)$ and negative $\nabla^2\rho(r)$ values at the BCPs. Also, the ϵ values at the BCPs were small and compatible with a normal single bond and the $E_d(r)$ yielded negative values, all of which also agrees with their being standard covalent molecules.

The numerical properties of the P−O BCPs for compounds **11** and **12** are listed in Table 2. The $\rho(r)$ has medium values (∼0.22 e/a_o^3) and the $\nabla^2\rho(r)$ is very large and positive (∼1.3 e/a_o^5). The ϵ was zero, evidencing the isotropy of the bond, compatible only with a single or triple bond but not with a double bond. The negative values of $E_d(r)$ indicated the stabilizing and attractive type of interaction in the bond. All these data are compatible with a very polarized bond. To study the exact type of interaction in the P−O bond, we found it necessary to analyze the $\nabla^2\rho(r)$, and in Figure 5 a contour map of the $\nabla^2\rho(r)$ is presented together with the zero flux surface and molecular graphs (a), and perspective view of the molecule, including the maxima on $\nabla^2\rho(r)$ around the VSCC of P and O

Table 3. Electronic Charge Density ($\rho(r)$), Laplacian of the Charge Density ($\nabla^2\rho(r)$), and Geometrical Disposition of the X and Z Atoms Maxima for $-\nabla^2\rho(r)$ in the VSCC, at the Different Theoretical Levels for Structures **7**−**19**

	$\rho(r)$ (e/a_o^3)		$\nabla^2\rho(r)$ (e/a_o^5)		dfp (Å)[b]		distance (Å)[c]	
maxima[a]	B3LYP	MP2	B3LYP	MP2	B3LYP	MP2	B3LYP	MP2
				7 (H_3NO) at O				
p1[d]	0.948	0.934	−5.228	−5.152	0.038	0.042	0.342	0.343
p2	0.456	0.467	−0.272	−0.346			0.448	0.442
				7 (H_3NO) at N				
p4[d]	0.510	0.514	−2.351	−2.461			0.426	0.425
p3	0.490	0.482	−1.915	−1.895			0.422	0.424
				8 (Me_3NO) at O				
p1[d]	0.936	0.920	−5.041	−4.952	0.040	0.043	0.343	0.345
p2	0.492	0.506	−0.479	−0.573			0.432	0.427
				8 (Me_3NO) at N				
p4[d]	0.481	0.482	−1.983	−2.034			0.423	0.423
p3	0.484	0.477	−1.900	−1.863			0.424	0.426
				9 (H_3NS) at S				
p1[d]	0.193	0.192	−0.514	−0.529	0.063	0.065	0.692	0.692
p2	0.127	0.131	−0.016	−0.018			0.811	0.816
				9 (H_3NS) at N				
p4[d]	0.507	0.508	−2.279	−2.336			0.428	0.431
p3	0.488	0.486	−1.957	−1.996			0.413	0.414
				10 (Me_3NS) at S				
p1[d]	0.191	0.189	−0.499	−0.506	0.075	0.075	0.693	0.694
p2	0.138	0.145	−0.066	−0.076			0.796	0.798
				10 (Me_3NS) at N				
p4[d]	0.473	0.473	−1.859	−1.888			0.427	0.427
p3	0.484	0.480	−1.982	−2.000			0.414	0.416
				11 (H_3PO) at O				
p1[d]	0.847	0.838	−3.722	−3.689	0.094	0.102	0.350	0.351
				11 (H_3PO) at P				
p4[d]	0.176	0.178	−0.522	−0.548			0.874	0.862
				12 (Me_3PO) at O				
p1[d]	0.841	0.832	−3.634	−3.610	0.106	0.114	0.351	0.351
				12 (Me_3PO) at P				
p4[d]	0.170	0.174	−0.424	−0.445			0.822	0.827
				13 (H_3PS) at S				
p1[d]	0.176	0.175	−0.406	−0.416	0.057	0.054	0.701	0.699
p2	0.175	0.177	−0.256	−0.265			0.771	0.772
				13 (H_3PS) at P				
p4[d]	0.175	0.177	−0.504	−0.531			0.877	0.862
p3	0.165	0.167	−0.315	−0.336			0.797	0.795
				14 (Me_3PS) at S				
p1[d]	0.175	0.173	−0.395	−0.401	0.076	0.072	0.702	0.702
p2	0.179	0.181	−0.286	−0.295			0.763	0.764
				14 (Me_3PS) at P				
p4[d]	0.168	0.172	−0.407	−0.430			0.821	0.825
p3	0.165	0.167	−0.330	−0.343			0.798	0.798
				15 (H_3AsO) at O				
p1[d]	0.868	0.852	−4.090	−3.962	0.054	0.067	0.348	0.349
				16 (Me_3AsO) at O				
p1[d]	0.859	0.845	−3.959	−3.857	0.062	0.075	0.349	0.350
				16 (Me_3AsO) at As				
p4[d]	0.234	0.239	−0.630	−0.677			1.435	1.409
				17 (H_3AsS) at S				
p1[d]	0.178	0.176	−0.413	−0.422	0.066	0.068	0.699	0.699
p2	0.154	0.155	−0.177	−0.182			0.764	0.765
				17 (H_3AsS) at As				
p3	0.153	0.155	−0.177	−0.182			1.319	1.300
				18 (Me_3AsS) at S				
p1[d]	0.176	0.174	−0.401	−0.407	0.081	0.082	0.700	0.701
p2	0.158	0.160	−0.207	−0.213			0.758	0.771
				18 (Me_3AsS) at As				
p4[d]	0.230	0.235	−0.607	−0.652			1.436	1.407

Table 3. (Continued)

	$\rho(r)$ (e/a_o^3)		$\nabla^2\rho(r)$ (e/a_o^5)		dfp (Å)[b]		distance (Å)[c]	
maxima[a]	B3LYP	MP2	B3LYP	MP2	B3LYP	MP2	B3LYP	MP2
				19 (F_3NO) at O				
p1[d]	0.876	0.860	−4.175	−4.081	0.099	0.116	0.347	0.348
p2	0.709	0.725	−1.829	−1.974			0.407	0.401
				19 (F_3NO) at N				
p4[d]	0.414	0.408	−1.337	−1.324			0.425	0.425
p3	0.630	0.623	−2.536	−2.374			0.418	0.421

[a] See Figure 4 for a definition of the maxima (p1, p2, p3, p4). [b] Distance from the three-maxima plane to the corresponding Z atom, see Figure 4 for a definition. [c] Distance from the maxima to the corresponding atom. [d] This BCP has two additional equivalent BCP.

Table 4. Bader's Atomic Charges and Dipole Moment (μ) for Structures **7**−**19** at the Different Theoretical Levels[a]

		charges		dipole moment (μ)		
		B3LYP	MP2	B3LYP	MP2	expt
7 (H_3NO)	at N	−0.41	−0.45	5.71	6.00	
	at O	−0.67	−0.71			
	at H	0.36	0.39			
8 (Me_3NO)	at N	−0.43	−0.48	5.05	5.26	5.45[b]
	at O	−0.70	−0.74			
	at C	0.20	0.17			
9 (H_3NS)	at N	−0.92	−0.99	6.33	6.43	
	at S	−0.32	−0.31			
	at H	0.41	0.43			
10 (Me_3NS)	at N	−0.91	−0.98	5.82	5.92	
	at S	−0.32	−0.38			
	at C	0.22	0.18			
11 (H_3PO)	at P	2.77	2.94	4.10	4.18	
	at O	−1.39	−1.40			
	at H	−0.46	−0.51			
12 (Me_3PO)	at P	2.96	3.18	4.65	4.66	4.29[b]
	at O	−1.43	−1.45			
	at C	−0.67	−0.81			
13 (H_3 PS)	at P	1.84	2.03	4.11	4.28	
	at S	−0.57	−0.61			
	at H	−0.43	−0.48			
14 (Me_3PS)	at P	2.08	2.35	5.19	5.17	4.73[b]
	at S	−0.68	−0.73			
	at C	−0.65	−0.79			
15 (H_3AsO)	at As	1.63	1.69	4.47	4.54	
	at O	−1.04	−1.06			
	at H	−0.20	−0.21			
16 (Me_3AsO)	at As	1.78	1.93	5.29	5.30	5.12[b]
	at O	−1.10	−1.12			
	at C	−0.41	−0.52			
17 (H_3AsS)	at As	1.12	1.17	4.28	4.39	
	at S	−0.57	−0.59			
	at H	−0.18	−0.19			
18 (Me_3AsS)	at As	1.30	1.45	5.59	5.56	5.14[b]
	at S	−0.67	−0.70			
	at C	−0.40	−0.50			
19 (F_3NO)	at N	1.07	1.12	0.31	0.69	0.039[c]
	at F	−0.25	−0.27			
	at O	−0.32	−0.32			

[a] All with 6-311+G* basis set as described in Methods section. [b] Values obtained in benzene from ref 90. [c] Gas-phase values from ref 91.

atoms (b) for compounds **11** and **12**. Also, the numerical values for the maxima in $\nabla^2\rho(r)$ are presented in Table 3.

Three maxima were found in the charge concentration over the VSCC, for each of the P and O atoms. The three maxima on the P atom correspond to the three bonded P−H bond maxima. The three on oxygen were staggered relative to the three P−H or P−C bonds (see Figure 4), and are directed in an almost trigonal disposition around the oxygen and away from the P and O atoms. The angle between these charge concentrations and the oxygen is around 113°. Numerically, no maxima could be found on the P−O axis between the P and O atoms. However, an electron density concentration (negative $\nabla^2\rho(r)$ values) was found around this axis, but in the O atom basin. The VSCC of phosphorus has almost disappeared and only a minor part of charge concentration of P−H bond remains in the basin of phosphorus (see Figure 5a,b). No maximum of charge concentration was found along the P−O axis away from oxygen (neither numerically nor graphically). This $\nabla^2\rho(r)$ topology around the P−O bond is compatible with a highly polarized bond, with an almost ionic σ bond (all the electron charge concentration ($-\nabla^2\rho(r)$) in the P−O bond belonged to the oxygen). This last fact agrees with the charges obtained by integration over the different atoms (see Table 4). Thus, the charge was ∼−1.4 on the oxygen atom basin, and ∼2.9 on the phosphorus. The hydrogens also had negative charge, in agreement with the $\nabla^2\rho(r)$ representation (see Figure 5). This charge distribution on the molecule accounts for the moderate dipole moment values for phosphine oxide derivatives (∼4.5 D).

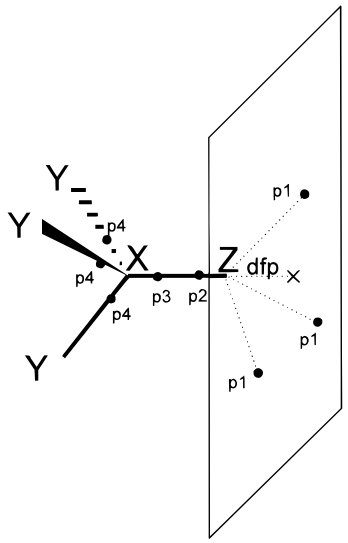

Figure 4. Definition of the distance (dfp) from Z atom to the plane formed by the three maxima, and definition of the maxima in $\nabla^2\rho(r)$ (p1, p2, p3, p4), for Y_3XZ molecules.

From the data described above for compounds **11** and **12**, we propose the following P−O bond nature: a strongly polarized σ bond (almost ionic) and three electron pairs on oxygen in a staggered distribution relative to P−H/P−C bonds as in scheme ii. It is uncertain at this stage whether there are additional π interactions between these three electron pairs on oxygen and the P atom.

C. Nature of the N−O Bond and Comparison with P−O. Tables 2 and 3 include results from calculations on ammonia oxide (**7**), its trimethyl derivative (**8**), and trifluoroamine oxide (**19**). The N−O bond in amine oxides is usually described[1,2,8,15,40] as a single semipolar bond with no back-bonding equivalent to the representation $R_3N^+-O^-$. The $\rho(r)$ and $\nabla^2\rho(r)$

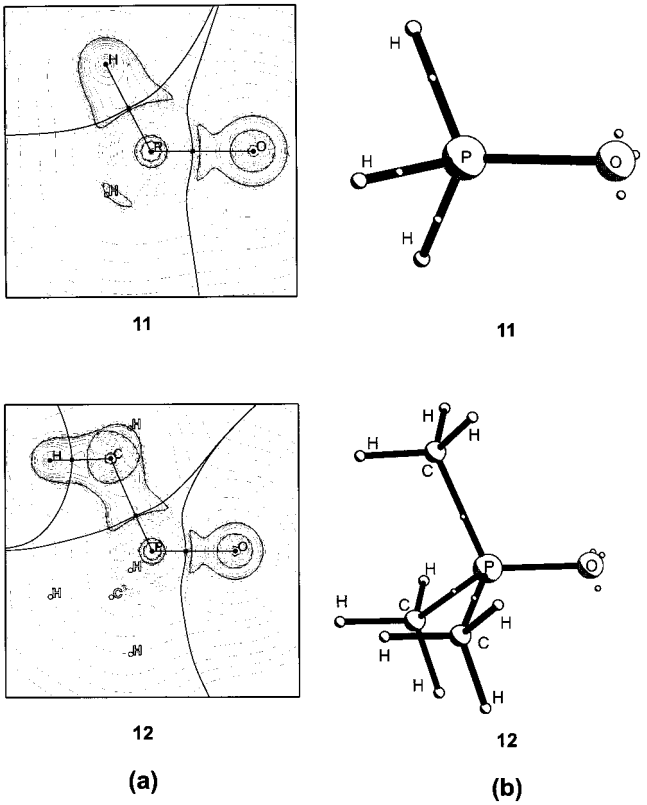

Figure 5. (a) Laplacian of ρ contour map, in the molecular plane obtained using the MORPHY program.[68] The contours begin at zero and they increase (solid contours) and decrease (dashed contours) in steps of $\pm 2 \times 10^n$, $\pm 4 \times 10^n$, and $\pm 8 \times 10^n$, with n beginning at -3 and increasing in steps of unity. The thick solid lines represent the molecular graph that joins the nuclei (solid circles) and the BCP (solid squares), and also represent the zero flux surface. (b) Perspective views including the maxima in $-\nabla^2\rho(r)$ on P and O atoms.

topological analyses gave the following results: the N−O bond was a covalent bond with ∼0.34 e/a_o^3 and ∼−0.22 e/a_o^5 values for the $\rho(r)$ and $\nabla^2\rho(r)$ respectively at its BCPs. The ϵ was zero and the $E_d(r)$ was ∼−0.3 (see Table 2). The graphical analysis of $\nabla^2\rho(r)$ showed (see Figure 6a) the electron density concentration located in the bond region, mainly in the nitrogen basin, but with a net electronic density donated to the oxygen basin. All the above is consistent with the semipolar single-bond description. Figure 6b depicts the perspective views of **7**, **8**, and **19**, together with the maxima on the $\nabla^2\rho(r)$ on oxygen and nitrogen atoms. Three maxima in $\nabla^2\rho(r)$ were found on the oxygen atoms for the three compounds. The disposition and orientation of the three maxima for compounds **7** and **8** were very similar to those for compounds **11** and **12**, discussed previously in Section III.B.

The N−O bond in amine oxides is generally accepted as a single bond without donor back-bonding in accord with the N−O bond theoretical distance (∼1.36 Å). However, it is generally accepted[44,77] that the N−O bond in F_3NO does contain

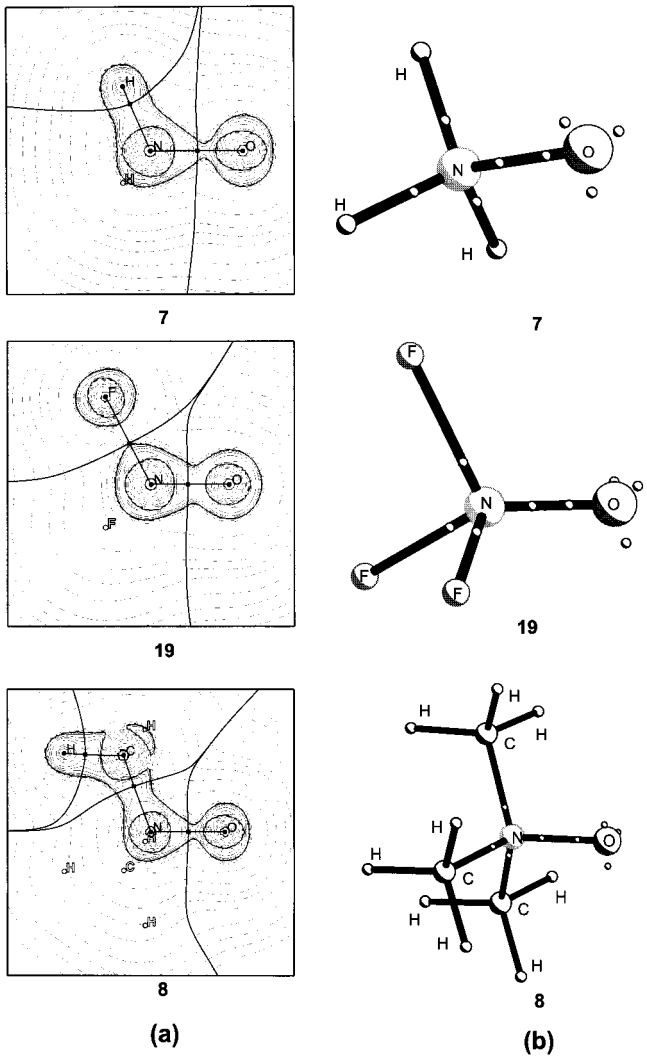

Figure 6. (a) Laplacian of ρ contour map, in the molecular plane obtained using the MORPHY program.[68] The contours begin at zero and they increase (solid contours) and decrease (dashed contours) in steps of $\pm 2 \times 10^n$, $\pm 4 \times 10^n$, and $\pm 8 \times 10^n$, with n beginning at -3 and increasing in steps of unity. The thick solid lines represent the molecular graph that joins the nuclei (solid circles) and the BCP (solid squares), and also represent the zero flux surface. (b) Perspective views including the maxima in $-\nabla^2\rho(r)$ on N and O atoms.

π back-donation, which is responsible for the extremely short bond distance. Our theoretical N−O distance for F_3NO was ∼1.15 Å in very good agreement with the experimental data and the previous theoretical result (Table 1). The numerical properties in the N−O BCP in **19** indicated a more covalent bond than in the amine oxides with the larger values of $\rho(r)$, $\nabla^2\rho(r)$, $E_d(r)$ and λ_1/λ_3, all characteristic of a very strong covalent bond. The $\nabla^2\rho(r)$ representation (see Figure 6a) displays a large electron density concentration in the N−O bond

(77) Grein, F.; Lawlor, L. *Theor. Chim. Acta* **1983**, *63*, 161.
(78) Lide, D. R.; Mann, D. E. *J. Chem. Phys.* **1958**, *29*, 914.
(79) Wilkins, C. J.; Hagen, K.; Hedberg, L.; Shan, Q.; Hedberg, K. *J. Am. Chem. Soc.* **1975**, *97*, 6352.
(80) Hehre, W. J.; Radom, L.; Schleyer, P. v. R.; Pople, J. A. *Ab initio Molecular Orbital Theory;* Wiley-Interscience: New York, 1986.
(81) Harmony, M. D.; Laurie, V. W.; Kuczkowski, R. L.; Schwendeman, R. H.; Ramsay, D. A.; Lovas, F. J.; Lafferty, W. J.; Maki, A. O. *J. Phys. Chem. Ref. Data* **1979**, *8*, 619.
(82) Chu, F. Y.; Oka, T. *J. Chem. Phys.* **1974**, *60*, 4612.
(83) Bartell, L. S.; Brockway, L. O. *J. Chem. Phys.* **1960**, *32*, 512.
(84) Jacob, E. J.; Samdal, S. *J. Am. Chem. Soc.* **1977**, *99*, 5656.
(85) Caron, A.; Palenik, G. J.; Goldish, F.; Donohue, J. *Acta Crystallogr.* **1964**, *17*, 102.
(86) Haaland, A.; Thomassen, H. *J. Mol. Struct.* **1991**, *263*, 299.
(87) Engelhardt, L. M.; Raston, C. L.; Whitaker, C. R.; White, A. H. *Aust. J. Chem.* **1986**, *39*, 2151.
(88) Eller, P. G.; Corfield, P. W. R. *J. Chem. Soc., Chem. Commun.*, **1971**, 105.
(89) Plato, V.; Hartford, W. D.; Hedberg, K. *J. Chem. Phys.* **1970**, *53*, 3488.
(90) (a) McClellan, A. *Tables of Experimental Dipole Moments*; Rahara Enterprises, 1973; Vol. 2. (b) McLellan, A. *Tables of Experimental Dipole Moments*; Rahara Enterprises, 1989; Vol. 3.
(91) Nelson, R. D. ; Lide, D. R.; Maryott, A. A. *Natl. Stand. Ref. Data Ser.−Natl. Bur. Stnds.* **1967**, *10*.

region. Table 3 and Figure 6b) show the three maxima on the O atom staggered with respect to the three F−N bonds. In this case, a fourth maximum on oxygen (along the N−O axis) was also found, but with lower $\rho(r)$ and $\nabla^2\rho(r)$ values. The issue of whether π back-donation exists for F_3NO can be studied by analyzing the position of the three electron pairs on the O atom. If a π interaction exists, the centroids of the electron pairs on the O atom should shift in some way toward nitrogen. In Table 3 the distances of the three-maxima plane (dfp)(for definition see Figure 4) to the corresponding atoms are compared. The distance for the N−O bond in **7** and **8** was around 0.04 Å, whereas this distance for the N−O bond in **19** was 0.1 Å, quite similar to the distance of the three-maxima plane to oxygen in phosphine oxides. In other words, for F_3NO, the three electron pairs on oxygen did not approach the nitrogen, but rather moved away. In addition, the distances of the maxima to the O atom were 0.342 Å for the amine oxide, and 0.347 Å for the F_3NO (see Table 3). Consequently, the angle between the nonbonded electron pairs and the O atom decreased in F_3 NO in comparison to amine oxide (113 vs 118°, see Figure 6). The existence of π back-bonding in the F_3NO is inconsistent with the above geometrical features of the electron maxima concentration of oxygen. Thus we conclude that there is no π back-donation in F_3NO bonding, as is generally true for all the X−O (X = N, P, As) bonds presented in this work. The different nature of the N−O and P−O bonds is included in the following description: *there is a polar single σ bond which has characteristics determined mainly by electrostatic interactions.*

This can be used to explain the observed experimental phenomenon of the low dipole moment of phosphine oxides, the strength of the P−O bond, and the difference between H_3NO and F_3NO. Thus, the amount of electrostatic interaction for the different X−O bonds is readily determined by using Bader atomic charges obtained by integration over atomic basins. These charges are listed in Table 4 for compounds **7**−**19**. The charge distribution in **11** (−1.4 on O and 2.9 on P) implies a strong electrostatic attraction strengthening the P−O bond. The hydrogen basins yielded negative charges contributing to a moderate overall dipole moment. Ammonia oxide **7** has negative charge on the N and O (∼−0.4 on N and −0.7 on O). Consequently there is electrostatic repulsion between them, producing a longer bond (1.36 Å). The hydrogens are positively charged, and the overall charge distribution yields a large dipole moment (∼6 D). The electronic charge distribution over the basins in F_3NO is dramatically different with a medium negative charge on the oxygen and fluorine atoms, and a positive charge on nitrogen. Therefore, an electrostatic attraction exists between the nitrogen and oxygen atoms, giving shorter bonds. On the other hand, the negative charge is distributed over oxygen and fluorine atoms producing a very low dipole moment (between 0.3 and 0.7 D).

D. Bonding in X−O,S Systems. To test the validity of the bonding scheme proposed here, we studied the As−O and X−S (X = N, P, As) bonding also.

In arsine oxide and its trimethyl derivative (**15** and **16**), the As−O bond was around 1.65 Å, shorter by 0.18 Å than the normal single As−O bond in **22** (see Table 1). This shows substantial strength in the As−O bond. Arsine oxides also yielded a highly polar As−O bond. The BCPs in $\rho(r)$ showed medium values of $\rho(r)$ and large and positive $\nabla^2\rho(r)$ (∼0.6 e/a_o^5). The ϵ was zero. The λ_1 and λ_3 ratio was around 0.26, showing a strongly polar, almost an ionic bond in agreement with the $\nabla^2\rho(r)$ contour map (see Figure 8). In this figure the VSCC of the arsenic atom has almost disappeared for compounds **15** and **16**, giving all the electron density concentration of the As−O bond located in the O basin. Looking for the maxima in the electron density concentration around oxygen, we found once again three equivalent and symmetrically distributed electron pairs on oxygen, staggered with respect to the As−H/As−C bonds. The electron density concentration on the As−O bond was found graphically but no local maxima were found numerically. The disposition of the three electron pairs on oxygen was quite similar to those previously described for amine and phosphine oxides (see Figure 8). The distance of the three-maxima plane to oxygen was 0.06 Å, intermediate between the same distances in amine and phosphine oxides. The charges over the atom basins in compounds **15** and **16** showed a highly polar bond and explain the large electrostatic interactions between As and O atoms. Thus, the charge on oxygen was large and negative (∼−1.1). The charge on arsenic was very large and positive (∼1.7), and the charges on the hydrogen

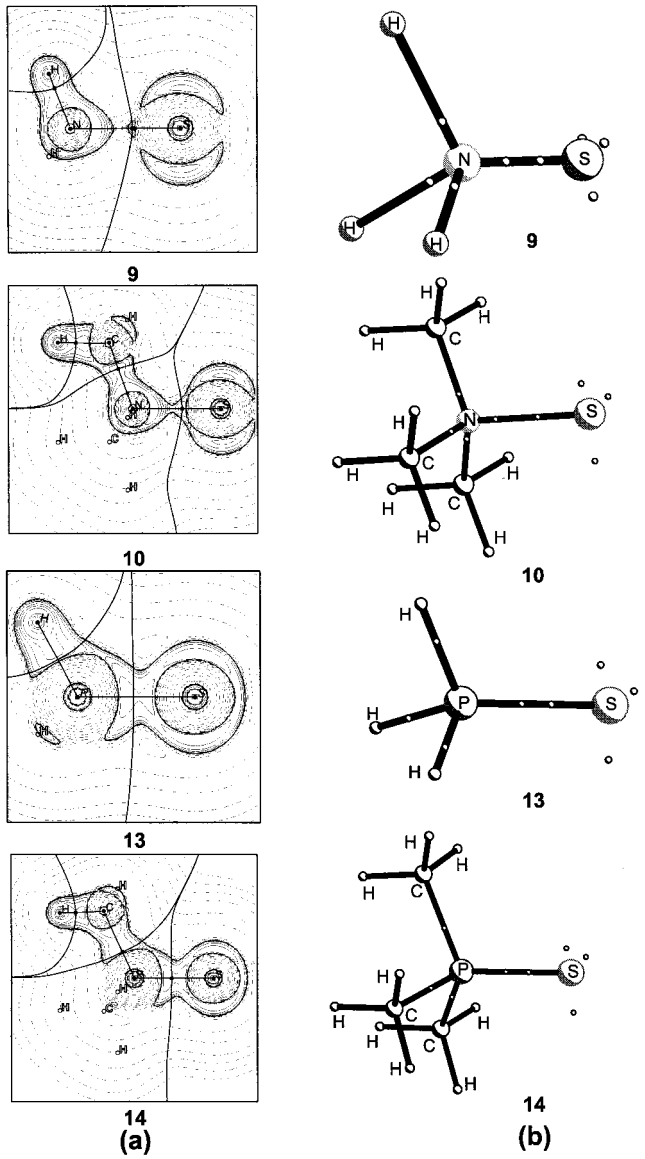

Figure 7. (a) Laplacian of ρ contour map, in the molecular plane obtained using the MORPHY program.[68] The contours begin at zero and they increase (solid contours) and decrease (dashed contours) in steps of $\pm 2 \times 10^n$, $\pm 4 \times 10^n$, and $\pm 8 \times 10^n$, with n beginning at −3 and increasing in steps of unity. The thick solid lines represent the molecular graph that joins the nuclei (solid circles) and the BCP (solid squares), and also represent the zero flux surface. (b) Perspective views including the maxima in $-\nabla^2\rho(r)$ on N, P, and S atoms.

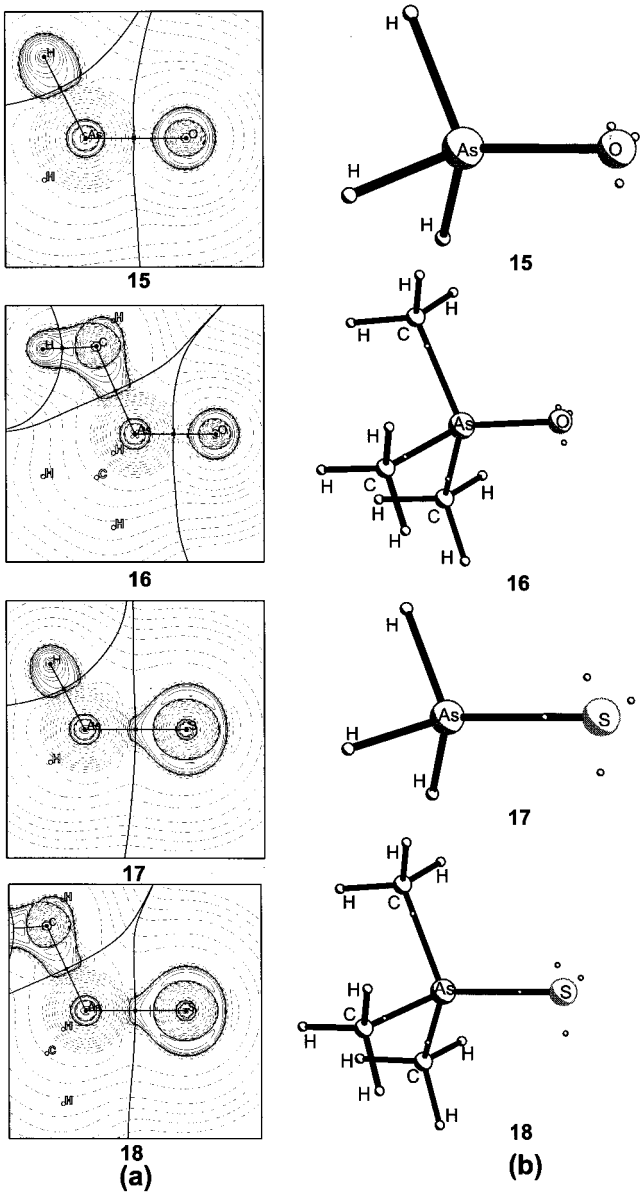

Figure 8. (a) Laplacian of ρ contour map, in the molecular plane obtained using the MORPHY program.[68] The contours begin at zero and they increase (solid contours) and decrease (dashed contours) in steps of $\pm 2 \times 10^n$, $\pm 4 \times 10^n$, and $\pm 8 \times 10^n$, with n beginning at -3 and increasing in steps of unity. The thick solid lines represent the molecular graph that joins the nuclei (solid circles) and the BCP (solid squares), and also represent the zero flux surface. (b) Perspective views including the maxima in $-\nabla^2\rho(r)$ on As, O, and S atoms.

basins were small and negative (~ -0.2). This charge distribution accounted for the electrostatic bond interaction and the moderate dipolar moments for arsine oxides (very similar to phosphine oxide). All these observations agree with the proposed bond nature.

The scheme was also extended to X−S bonds (X = N, P, or As) (**9**, **10**, **13**, **14**, **17**, and **18**). Compounds **9** and **10** presented a general behavior similar to **7** and **8** but with minor differences. The N−S bond is a polar coordinated bond with low amount of electron donation from the N to S atom. The $\rho(r)$ (0.13 e/a_o^3) in the N−S BCPs is small compared to the amine or phosphine oxides. The $\nabla^2\rho(r)$ also proved extremely small (< -0.02 e/a_o^5) (see Table 2). The ϵ remains zero and the $E_d(r)$ (~ -0.1 vs. -0.3) is smaller than the corresponding oxides. From Figure 7, the majority of the charge concentration is located on the nitrogen basin. All the above characteristics result in a weaker bond. The three maxima on sulfur adopt an orientation similar those previously found for oxygen, with a distance from the plane to the sulfur atom of around 0.07 Å. The bond length for the N−S bond is larger than the normal single bond, in compound **24** (1.83 and 1.732 Å, respectively). This lengthening is due mainly to the electrostatic interactions. Taking into account that **9** and **10** have small and negative charges on the S basin and large and negative charge on the nitrogen basins, the electrostatic repulsion should lengthen the bond. So, the overall electron distribution on the molecule yields a large dipole moments (>6 D).

Compounds **13**, **14**, **17**, and **18** presented an overall behavior similar to that of the phosphine oxides: the P−S and As−S bond lengths are shorter than the single P−S and As−S bonds in compounds **21** and **23** (see Table 1) and have medium $\rho(r)$ values on the BCPs. Moreover, the $\nabla^2\rho(r)$ proved negative but the numerical values for **17** and **18** were small in magnitude (~ -0.3 for **13** and **14** and ~ -0.1 e/a_o^5 for **17** and **18**). Invariably, the ϵ became zero, and the $E_d(r)$ for compounds **17** and **18** is negative and small (~ -0.08). From Figure 7, the electronic density concentration is located on the P−S bond between both basins for compounds **13** and **14**, showing the mainly covalent nature of the bond. This was also true for compounds **17** and **18** but the electron density concentration is located mainly on the sulfur basin (see Figure 8). The three electron pairs on sulfur show similar orientations to those found in phosphine and amine oxides. The three maxima main plane distance to the sulfur atom was between 0.5 and 0.8 Å. The charge distribution also resembles that obtained for phosphine oxide (negative charge on sulfur, large positive charge on the P or As atoms, and smaller negative charge on hydrogens). This electron distribution should be responsible for a large electrostatic attraction between S and P, or between S and As. On the other hand, the dipole moment for these compounds was also highly similar to that of phosphine oxide ($\sim$4.5 D).

In general, the X−Z bond nature of the compounds studied fits with the concept of a single σ bond with different polar nature (from almost an ionic to mainly a covalent bond) due to the electronegativity of the atoms involved, and with different electrostatic interactions, depending on the different basin charge distribution that strengthens or weakens the corresponding bond. One last issue on the covalent nature of the X−Z bond was tested by looking at the λ_1/λ_3 values (see Table 2). The almost ionic bonds showed extremely small values ($\sim$0.2 for compounds **11** and **12** and **15** and **16**) while large values were shown by covalent bonds (> 0.6 for **7**, **8**, **13**, **14**, **17**, and **18**). Additional calculations are in progress to analyze the bonding in phosphonium ylides and some related compounds.

IV. Conclusions

A theoretical study of hypervalent compounds was carried out by DFT and MP2 methods. Both methods yielded similar results and agreed with the previous experimental and theoretical data.

The bonding nature of Y_3 XZ (Y = H or Me; X = N, P or As; Z = O or S) compounds has been analyzed using the *Atoms in Molecules Theory*. The analysis was performed using different wavefunctions from different levels of theory and basis sets. The quantitative and qualitative results obtained from the different wavefunctions were in strong agreement, suggesting that the Bader analysis was *level/basis set* independent, at the level of theoretical description chosen.

From the topological analyses performed, we propose that the XZ bond in the Y_3XZ series of molecules is a single, highly

polarized σ bond, with strength dependent on the electrostatic interactions between the X and Z atoms. This bonding nature is close to model ii proposed by Streitwieser et al.,[10,11] however, no π back-donation can clearly be found to arise from our results.

Acknowledgment. Computing time was provided by the *Universidad de Granada, Centro Informático Científico de Andalucía* (CICA) (Spain) and the *Centre of Scientific Computing* Espoo (Finland). We are grateful to Professor R. W. F. Bader for a copy of the AIMPAC package of programs and to Professor P. L. A. Popelier for a copy of the MORPHY program. We are also obliged to Neste Oy Research Foundation for a visiting scientist fellowship. We are grateful to the referees for their useful and constructive comments and suggestions. We thank David Nesbitt for corrections made to the original English manuscript. J.M.M. dedicates this work to Prof. F. J. López Aparicio and Prof. J. A. López Sastre.

Supporting Information Available: Table 5 containing the total energy (hartrees) for structures **1**−**24** (1 page, print/PDF). See any current masthead page for ordering information and Web access instructions.

JA980141P